GEOCHEMISTRY

Relatively oxidized fluids fed Earth's earliest hydrothermal systems

Dustin Trail[1]* and Thomas M. McCollom[2]

The properties of high-temperature lithospheric fluids within the early Earth are poorly known, yet many origin-of-life scenarios depend upon their characteristics. These fluids represent a key communication pathway between Earth's interior and hydrothermal pools. We use zircon chemistry, experiments, and modeling to infer the character of lithospheric fluids approaching 4 billion years. We constrain oxygen fugacity, chlorine content, and temperature, which allow us to model the solubility and transport of metals that are hypothesized to be crucial for the origin of life. We show that these fluids were more oxidized than the terrestrial mantle during this time and that they were interacting with near-surface aqueous systems, possibly subaerial hydrothermal pools, amplifying redox gradients in a location attractive for prebiotic molecular synthesis or sustained microbial activity.

High-temperature fluids constitute a bridge between the solid earth and shallow subsurface hydrothermal systems; i.e., they transport solubilized rock components to the surface. The properties of high-temperature lithospheric fluids are broadly constrained for the modern Earth, but the characteristics of these fluids during the first 700 million years of our planet's history remain largely unknown. The problem is that mineral proxies that can record subsolidus fluid-rock interactions during the Eoarchean and Hadean [>3.6 billion years (Ga) ago] are sparse or altogether absent, leaving the chemical and physical properties of hydrothermal fluids largely uncertain. In the past several years, key discoveries have revealed a handful of ~4-Ga-old zircons ($ZrSiO_4$) that record temperatures too low to be directly attributable to crystallization from igneous magma, and therefore must have formed from aqueous fluid interactions within the crust (*1*, *2*). This presents an opportunity to explore—by zircon proxy—the properties of ancient lithosphere fluids interacting with rock.

Here, we show that zircon trace-element and isotope characteristics frame a geologic environment where the fluids are connected to subaerial hydrothermal systems. We also present a zircon experimental calibration to quantify the oxygen fugacity (fO_2) of the fluid(s). When the calibration is applied to zircons approaching 4 Ga old, it reveals oxidized conditions relative to recent high-precision fO_2 sensors applied to mantle rocks of similar age (*3*). The fO_2 is an important variable to quantify because it affects the stability of minerals, as well as the composition of the coexisting fluid. For redox-sensitive elements (e.g., Fe, Zn, S, C), fO_2 also regulates the solubility and speciation of the constituents in the fluid. Moreover, an enormous amount of geochemical energy is potentially available from redox disequilibria that may arise during buoyant fluid transport and chemical interactions between the solid earth and surface fluids. When available chemical constraints are considered, our preferred model is that relatively oxidized hydrothermal fluids fed subaerial hydrothermal pools nearly 4 Ga ago. Complementary geochemical rock-fluid modeling reveals that Mn, Zn, and Fe were more available than Cu to participate as inorganic metal catalysts in prebiotic chemistry or to support an already established biome if life was present.

[1]Department of Earth and Environmental Sciences, University of Rochester, Rochester, NY 14627, USA. [2]Laboratory for Atmospheric and Space Physics, University of Colorado, Boulder, CO 80309, USA.
*Corresponding author. Email: dtrail@ur.rochester.edu

Oxidation state of hydrothermal fluids

As a first step, we constrain fluid oxidation state using zircon chemistry as a proxy. In terrestrial systems, Ce is found as either a trivalent or tetravalent cation, with the latter exhibiting better compatibility in the Zr^{4+} site of zircon. The more oxidized the fluid, the greater the fraction of Ce^{4+} in the system, the consequence of which is a higher concentration of Ce in zircon. This is quantified through a partition coefficient, which represents the concentration of Ce in zircon divided by the Ce concentration in the fluid ($D_{Ce}^{zrc/fluid}$). Zircon-fluid partitioning experiments (fig. S1) were conducted as a function of fO_2 and temperature for Ce and other non–redox sensitive trivalent rare earth elements (REEs) (e.g., La, Pr, Sm, etc.). The Ce compatibility in zircon is presented relative to neighboring REEs by calculating a Ce anomaly:

$$\left(\frac{Ce}{Ce^*}\right)_D = \frac{D_{Ce}^{zircon/fluid}}{\sqrt{D_{La}^{zircon/fluid} \times D_{Pr}^{zircon/fluid}}} \quad (1)$$

where the subscript "D" indicates that the Ce anomaly is calculated with the partition coefficients. The Ce anomaly represents the deviation from a ~Ce^{3+}-only system. The Ce^{3+}-only partition coefficient is represented by the denominator of Eq. 1 and requires $D_{La}^{zrc/fluid}$ and $D_{Pr}^{zrc/fluid}$ to quantify. As defined, the higher the fO_2, the larger the Ce anomaly becomes in zircon. Five different fO_2 buffers were imposed upon zircon-fluid REE partitioning experiments to characterize the zircon Ce anomaly as a function of fO_2 and T (fig. S1), resulting in the following empirical calibration:

$$\log\left[\left(\frac{Ce}{Ce^*}\right)_D - 1\right] = (0.237 \pm 0.040) \times \log(fO_2) + \frac{9437 \pm 640}{T(K)} - 5.02 \pm 0.38 \quad (2)$$

If $(Ce/Ce^*)_D = 1$ (Eq. 1), the presence of only Ce^{3+} is implied, and so a Ce redox exchange reaction cannot be written, and the fO_2 cannot be calculated. More generally, if $(Ce/Ce^*) \leq 1$, the result is undefined, which is reflected by the term on the left-hand side of Eq. 2. We apply this calibration to detrital zircons from the Jack Hills, Western Australia, with crystallization temperatures below the granite solidus (*1*). The relative fO_2 for the fluids is reported with respect to the fayalite-magnetite-quartz (FMQ) equilibrium. That is, ΔFMQ is defined as the $\log_{10}[fO_2(\text{fluid})] - \log_{10}[fO_2(\text{FMQ})]$ at the zircon crystallization temperature. The fluid fO_2 ranges from ΔFMQ = 0.2 to 2.1, with an average ΔFMQ value of 1.1 (±0.6, 1 SD) (Fig. 1, A and B). These eight zircons were formed under unexpectedly oxidizing conditions and furthermore represent the oldest quantified fO_2 of terrestrial fluids, with U-Pb ages from 3840 to 3910 million years.

Subaerial environments on early Earth

Complementary chemical tracers (Fig. 1) help frame a local geologic environment. First, we emphasize that the above-mentioned zircons formed 50° to 100°C lower than magma solidification temperatures (Fig. 1C) (*4*). Second, $[Cl]_{zircon}$ and $D_{Cl}^{zrc/fluid}$ (*1*) give an average $[Cl]_{fluid}$ ~3 times lower than that of modern seawater (Fig. 1D). The salinity of Archean seawater and submarine hydrothermal fluids is thought to be comparable to modern values or higher (*5*, *6*), providing geochemical support that these zircons formed outside of a submarine environment. Thus, to explain $[Cl]_{fluid}$ values requires another source of fluids, such as meteoric water or volatile inputs from magma sources (*7*, *8*). Third, the local environment is further constrained from the zircon $\delta^{18}O$ values (*1*, *9*). Some grains are depleted in ^{18}O relative to zircon derived from mantle melts (*10*), a chemical feature that is consistent with input of meteoric water into the system. Similar oxygen isotope signatures, resulting from assimilation of crust that has been hydrothermally altered by surface waters, are

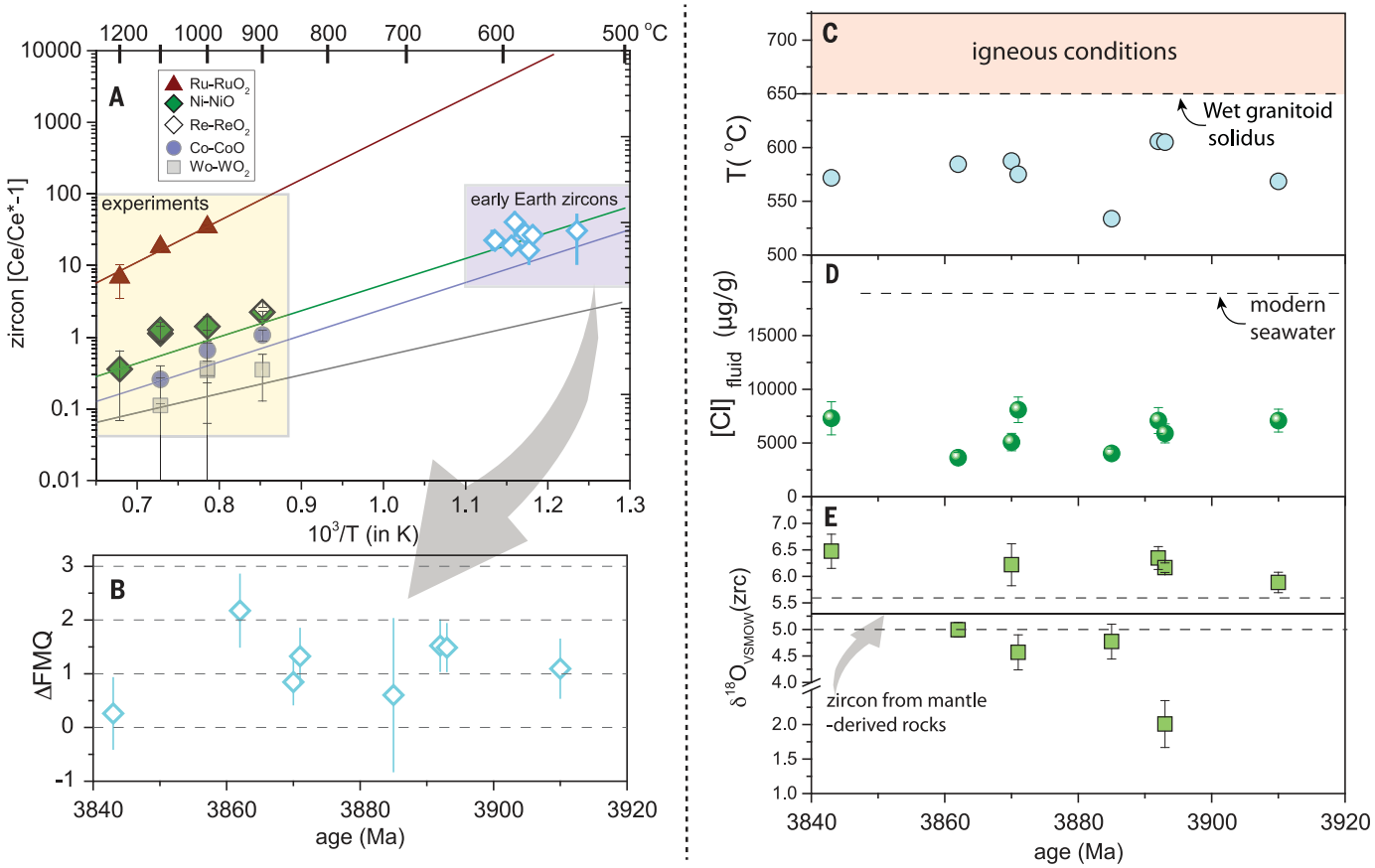

Fig. 1. Zircon trace-element and stable-isotope data. (**A**) Experimental calibration showing zircon Ce anomalies (plotted as Ce/Ce* − 1) for zircon-fluid REE partitioning from 16 experiments using five different metal-metal oxide fo_2 buffers (tables S3 to S6). Ce anomalies are positively correlated with fo_2 and inversely correlated with temperature (T). To apply this calibration to natural samples, Ce anomalies for the Jack Hills zircons are calculated by normalizing to the chondritic uniform reservoir (*32*), and T is derived using the Ti-in-zircon thermometer (*33*). (**B**) The calculated fo_2 of the fluids is relatively oxidized, i.e., ΔFMQ = 1.1. (**C**) Ti-in-zircon crystallization temperatures (*33*) plot below the wet granite solidus indicative of a nonmagmatic environment; here, equal titania and silica activities are assumed to calculate temperature (*1*, *9*). (**D**) Calculated fluid Cl content ($[Cl]_{fluid}$) using the measured Cl content in natural zircons ($[Cl]_{zircon}$) and zircon-fluid partitioning for Cl (*1*) give average values for $[Cl]_{fluid}$ of 6000 ± 1600 µg/g (1 SD; µg/g = mg/liter). (**E**) The $\delta^{18}O_{VSMOW}(zrc)$ values are defined as $([^{18}O/^{16}O]_{zircon}/[^{18}O/^{16}O]_{VSMOW} - 1) \times 1000‰$, where VSMOW is the Vienna standard mean ocean water standard.

Fig. 2. A model geologic environment, constrained by zircon chemistry. Hydrothermal fields, driven by magmatic heat, are replenished by meteoric water (*4*). The meteoric water is responsible for the subset of the zircons with submantle $\delta^{18}O$ values (Fig. 1E), and low $[Cl]_{fluid}$ when compared to seawater (Fig. 1D). Both are indicators of subaerial environments. Zircons with $\delta^{18}O$ values above that of the mantle field (Fig. 1E) interacted with a comparatively smaller fraction of meteoric water, possibly owing to formation at greater depths (*7*). Hydrothermal activity can last >10^6 years; systems may wane, followed by rejuvenation with later magma pulses (*34*).

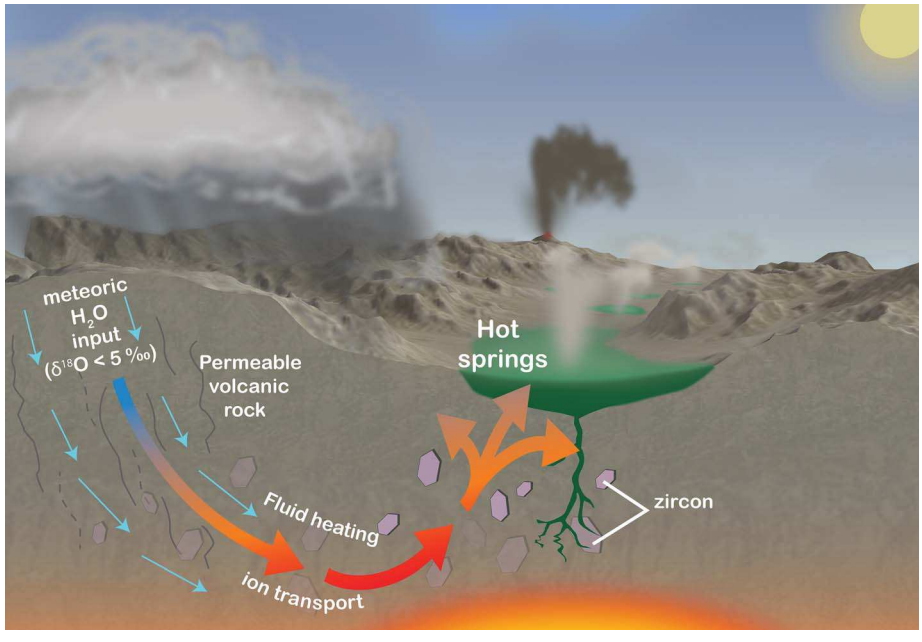

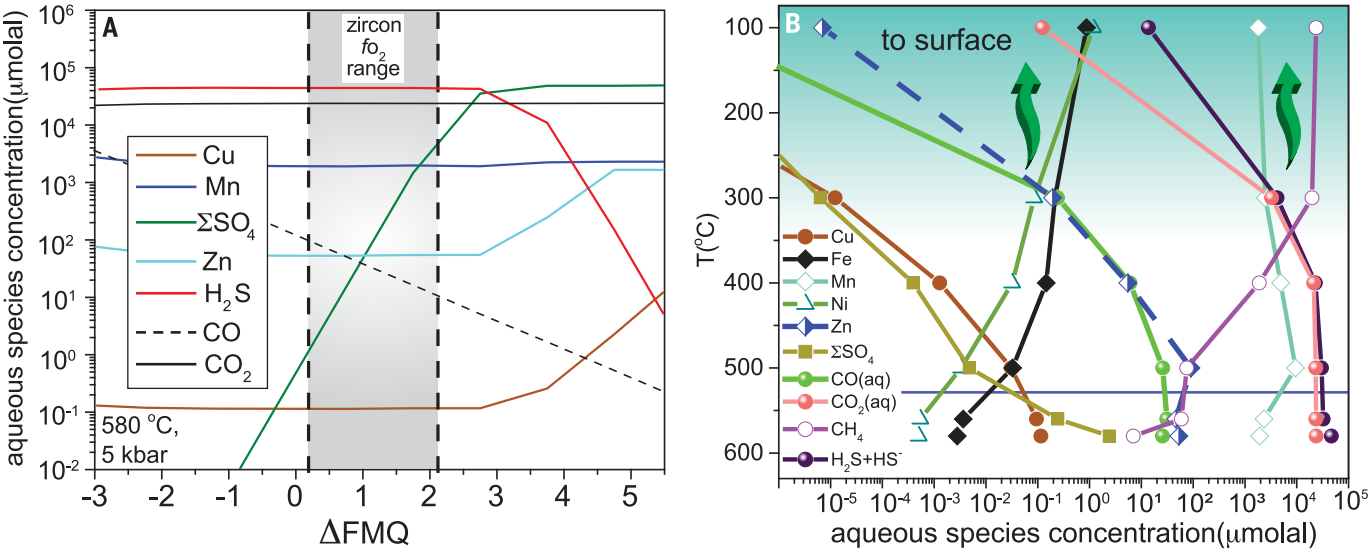

Fig. 3. Early Earth fluid properties determined from reaction path models. (**A**) Predicted equilibrium abundances of total dissolved metals, carbon, and sulfur species from the models constrained by zircon chemistry. Sulfate-bearing species are present across the entire fo_2 range predicted here, though the total concentration ($\sum SO_4$) decreases by about three orders of magnitude across this range. Not shown are Fe and Ni, whose concentrations are $<10^{-2}$ μmolal (*4*) and are thus off the scale. (**B**) A model that tracks metal solubility in the fluid during buoyant rise en route to the surface. Temperatures lower than the solid purple line (~530°C) are model extrapolations that extend to lower temperatures than the zircon data. These models were executed at average fo_2 values of ΔFMQ = 1 (*4*). Methane exhibits increasing abundance at lower *T*, reflecting the increased thermodynamic stability of reduced carbon species. At 100°C Cu, $\sum SO_4$, and CO(aq) plot off the scale and have respective concentrations of ~10^{-11}, ~10^{-9}, and ~10^{-8} μmolal. The models do not take into consideration that fluids that transition rapidly from high to low *T* may carry higher loads of dissolved solutes than those predicted by the discrete equilibrium steps. Also, the models do not take into consideration complexation of metals with organic compounds, which may inhibit the formation of metal precipitates at lower temperature near the surface and enhance the concentration of some dissolved metals in hydrothermal fluids (*35*).

common in modern hotspot settings such as Iceland and Yellowstone (*11*). Moreover, complementary ^{18}O-enriched and -depleted zircon, relative to the mantle (Fig. 1E), has also been argued to be a chemical feature of early Earth Iceland-like systems (*7*), similar to the environment that we propose here (*4*). To summarize, the zircon geochemistry requires relatively oxidized lithospheric fluids (~580°C), shallow subsurface water-rock interactions, fluid derived from meteoric sources, and restricted input of Cl-rich fluid into the source, where the latter two constraints are consistent with a subaerial environment (Fig. 2).

These fluid-rock interactions represent a more enclosed environment—compared to a substantially larger body of water such as a global ocean (*12*)—which likely helps concentrate and enhance the participation of metals in prebiotic reactions. To explore the behavior of metals, minerals, and other volatiles in the environment inferred above, we implement reaction path models using the software package EQ3/6 (*13*) to calculate equilibrium fluid and mineral compositions for a representative rock composition over a range of fo_2, $[Cl]_{fluid}$, and T (*4*). The starting rock is based on the average composition for icelandites from the GEOROC database (n = 123 rock samples, where the average SiO_2 content is 57.6 ± 5 wt %, 1 SD) (*4*).

We show the abundances of metals and predominant sulfur and carbon species from 580°C in models across a range of fo_2 conditions (Fig. 3A), with corresponding mineralogy and additional model results (fig. S2). Our modeling demonstrates that the three most abundant metals in the fluid (at 580°C) are Mn, Zn, and Cu. The dominant S-bearing species across the fo_2 range predicted by the zircon data is H_2S at 580°C, whereas the concentration of SO_4-bearing species ($\sum SO_4$) only dominates at fo_2 values more oxidizing than those predicted here (i.e., ΔFMQ ≥ 3). Carbon dioxide is two to three orders of magnitude more abundant than CO across the same fo_2 range. We now turn to a simple observation: Hot fluids are buoyant and lower in density than the rock in which they tend to interact. We now model the solubility changes with decreasing temperature and pressure during transport of the fluid to the surface (Fig. 3B).

Availability of metals for prebiotic chemistry

With these model results, we can infer the relative abundances of metals and explore the viability of their role in the local early Earth environment that may have been suitable for life or the emergence of life. This objective shares some commonalities with metallomics, a concept developed to recognize the importance of metal-assisted function in modern cellular reactions (*14*). For instance, enzyme metal cofactors such as Cu, Fe, and Zn are common in modern proteins (*15*), and some ribozymes require the presence of metal cations for catalysis (*16*). The metallome certainly evolved though time, regulated by metal availability owing to solid earth processes and biome feedback, resulting in amplified or muted biological function (*17*). The identity of metals associated with Paleoarchean carbonaceous residue, for example, has been used to infer ancient biological function and the chemical selectivity of ancient cells (*18*). Even further back in time, metal ions may have served an essential role as primitive catalysts (*19*) before life arose on Earth. Metals may thus function as key intermediaries between emerging biologic and prebiotic systems and the environment, providing strong motivation to explore metal-specific prebiotic paths using our results to provide context.

Copper-cyanometallates, for example, were shown to be a key component of one hypothesized reaction path for abiotic synthesis of glycolaldehyde and glyceraldehyde, under experimental conditions designed to emulate a subaerial environment exposed to ultraviolet radiation (*20*). However, our water-rock modeling yields very low Cu fluid concentrations that call into question the availability of Cu to catalyze the production of these simple sugars or other organic compounds (Fig. 3B).

On the other end of the spectrum, Mn has the highest concentration of metallic solutes inferred for the hydrothermal fluids (Fig. 3B), yet this metal is only rarely considered in origin-of-life scenarios (*21*). The high predicted $[Mn]_{fluid}$ is nevertheless consistent with Mn enrichments documented in the remains of younger subaerial Archean hot springs (*22*). Zinc and Ni concentrations are on the order of ~1 μmolal at 100° to 300°C (Fig. 3B), which is >5 orders of magnitude more abundant than Cu under the same conditions. Zinc, and to a minor extent Ni, are known to increase the adsorption of nucleotides and adenosine onto clays, and crucially, both elements are more effective at doing so than Na, Mg, and Ca, which are major cations in modern seawater (*23*). Enhanced Zn- and Ni-mediated absorption of biomolecules onto mineral surfaces can help concentrate simple organics for subsequent polymerization steps, potentially in the presence of sheet silicate minerals such as muscovite, tremolite, and prehnite, which all have stability fields that exist below 400°C (fig. S2).

The relatively oxidizing conditions seen in this study also result in a mixture of Fe^{2+} and Fe^{3+} in the fluid and minerals. At 580°C, magnetite ($Fe_2^{3+}Fe^{2+}O_4$) and pyroxenes are predicted to be the stable Fe-bearing minerals, whereas from 400° to 100°C epidote ($Ca_2Fe^{3+}Al_2Si_3O_{12}[OH]$) and annite ($KFe_3^{2+}AlSi_3O_{10}[OH]_2$) represent the equilibrium minerals. This is a key observation, given that the presence of mixed-valence Fe-hydroxides (versus Fe^{2+} or Fe^{3+} only) may enhance amino acid formation in synthetic hydrothermal vent systems (*24*). In addition, although Fe^{3+} is relatively insoluble in aqueous fluids, it is present with H_2S; both are thought to be requisites to form Fe-S clusters (*25*), hypothesized by some to be among the most ancient metal-based cofactors in primitive metabolic networks (*26*, *27*). Finally, methane becomes increasingly stable at lower temperatures; this component is frequently used as a reactant in experiments that seek to produce primitive prebiotic compounds, such as nucleic and amino acids (*28*).

With the model results presented (Fig. 3B), we assume an evolution of buoyant fluids along an f_{O_2} of ~ΔFMQ+1, independent of temperature, though hydrothermal systems are inherently in a state of disequilibrium and fluids may evolve along different f_{O_2} paths. We cannot exclude the possibility that fluids entered into a more reducing (or oxidizing) environment that is at or near the surface of Earth, which would produce a redox gradient. This intriguing scenario may also solve a paradox in prebiotic chemistry in which oxidizing and reducing conditions are "simultaneously" required (*29*) to increase molecular complexity to obtain prebiochemistry molecules such as aspartate and pyrimidines (*30*, *31*). Although the fluids constrained here would most likely represent a subset of the diversity of early terrestrial hydrothermal systems, our results mark the oldest quantified f_{O_2} of fluids in Earth's crust, which may have fed hydrothermal systems capable of concentrating and fractionating metals and other raw ingredients necessary for "productive" prebiotic activity.

REFERENCES AND NOTES

1. H. Tang, D. Trail, E. A. Bell, T. M. Harrison, *Geochem. Perspect. Lett.* **9**, 49–53 (2019).
2. T. M. Harrison, *Hadean Earth* (Springer, ed. 1, 2020).
3. L. Gao *et al*., *Nat. Commun.* **13**, 3283 (2022).
4. Materials and methods are available as supplementary materials.
5. B. Marty, G. Avice, D. V. Bekaert, M. W. Broadley, *C. R. Geosci.* **350**, 154–163 (2018).
6. R. Burgess *et al*., *Am. Mineral.* **105**, 1317–1325 (2020).
7. J. R. Reimink, T. Chacko, R. A. Stern, L. M. Heaman, *Nat. Geosci.* **7**, 529–533 (2014).
8. S. Arnórsson, A. Andrésdóttir, *Geochim. Cosmochim. Acta* **59**, 4125–4146 (1995).
9. E. A. Bell, T. M. Harrison, *Earth Planet. Sci. Lett.* **364**, 1–11 (2013).
10. J. W. Valley *et al*., *Contrib. Mineral. Petrol.* **150**, 561–580 (2005).
11. I. Bindeman *et al*., *Terra Nova* **24**, 227–232 (2012).
12. B. Damer, D. Deamer, *Astrobiology* **20**, 429–452 (2020).
13. T. J. Wolery, R. L. Jarek, *Software User's Manual: EQ3/6, Version 8.0* (Lawrence Livermore National Laboratory, 2003).
14. J. J. R. Fraústo da Silva, R. J. P. Williams, *The Biological Chemistry of the Elements: The Inorganic Chemistry of Life* (Oxford Univ. Press, ed. 2, 2001).
15. J. A. Tainer, V. A. Roberts, E. D. Getzoff, *Curr. Opin. Biotechnol.* **2**, 582–591 (1991).
16. R. K. O. Sigel, A. M. Pyle, *Chem. Rev.* **107**, 97–113 (2007).
17. A. L. Zerkle, C. H. House, S. L. Brantley, *Am. J. Sci.* **305**, 467–502 (2005).
18. K. Hickman-Lewis *et al*., *Sci. Rep.* **10**, 4965 (2020).
19. B. C. Clark, V. M. Kolb, *Life* **10**, 278 (2020).
20. D. Ritson, J. D. Sutherland, *Nat. Chem.* **4**, 895–899 (2012).
21. B. Bhushan, U. Shanker, Kamaluddin, *Orig. Life Evol. Biosph.* **41**, 469–482 (2011).
22. M. J. Van Kranendonk *et al*., *Astrobiology* **21**, 39–59 (2021).
23. J. Hao, M. Mokhtari, U. Pedreira-Segade, L. J. Michot, I. Daniel, *ACS Earth Space Chem.* **3**, 109–119 (2019).
24. L. M. Barge, E. Flores, M. M. Baum, D. G. VanderVelde, M. J. Russell, *Proc. Natl. Acad. Sci. U.S.A.* **116**, 4828–4833 (2019).
25. C. Bonfio *et al*., *Nat. Chem.* **9**, 1229–1234 (2017).
26. J. E. Goldford, H. Hartman, T. F. Smith, D. Segrè, *Cell* **168**, 1126–1134.e9 (2017).
27. E. K. Moore, B. I. Jelen, D. Giovannelli, H. Raanan, P. G. Falkowski, *Nat. Geosci.* **10**, 629–636 (2017).
28. T. M. McCollom, *Annu. Rev. Earth Planet. Sci.* **41**, 207–229 (2013).
29. S. A. Benner *et al*., *ChemSystemsChem* **2**, (2020).
30. G. D. Cody *et al*., *Geochim. Cosmochim. Acta* **68**, 2185–2196 (2004).
31. M. Yadav, R. Kumar, R. Krishnamurthy, *Chem. Rev.* **120**, 4766–4805 (2020).
32. D. Trail, E. B. Watson, N. D. Tailby, *Nature* **480**, 79–82 (2011).
33. J. M. Ferry, E. B. Watson, *Contrib. Mineral. Petrol.* **154**, 429–437 (2007).
34. E. Martin, O. Sigmarsson, *Lithos* **116**, 129–144 (2010).
35. S. G. Sander, A. Koschinsky, *Nat. Geosci.* **4**, 145–150 (2011).

ACKNOWLEDGMENTS

We thank Y. Wang, J. Buettner, and K. Johnston for technical assistance and three reviewers for constructive comments. **Funding:** This work was supported by NSF EAR-175190 and NASA grant 80NSSC19M0069. **Author contributions:** Conceptualization: D.T. Methodology: D.T., T.M.M. Investigation: D.T., T.M.M. Visualization: D.T., T.M.M. Funding acquisition: D.T., T.M.M. Project administration: D.T., T.M.M. Supervision: D.T., T.M.M. Writing – original draft: D.T. Writing – review and editing: D.T., T.M.M. **Competing interests:** The authors declare that they have no competing interests. **Data and materials availability:** All experimental data are available in the main text or the supplementary materials. EQ3/6 model outputs are included in the supplementary materials.

SUPPLEMENTARY MATERIALS

science.org/doi/10.1126/science.adc8751
Materials and Methods
Supplementary Text
Figs. S1 to S8
Tables S1 to S8
References (*36*–*57*)
Data S1

Submitted 5 May 2022; accepted 6 December 2022
10.1126/science.adc8751